Icarus 365 (2021) 114495

Contents lists available at ScienceDirect

Icarus

journal homepage: www.elsevier.com/locate/icarus

Quantifying misidentification rates of Europa's microfeatures in low-resolution Galileo imaging

J.L. Noviello [a,*], A.R. Rhoden [b]

[a] School of Earth and Space Exploration, Arizona State University, Bateman Physical Sciences, F-Wing 686, Tempe, AZ 85287, USA
[b] Southwest Research Institute, 1050 Walnut Street, Suite 300, Boulder, CO 80302, USA

ARTICLE INFO

Keywords:
Europa
Jupiter
Satellites
Geological processes

ABSTRACT

Europa is a compelling target because of its unique geology and potential for habitability. Efforts to map the small-scale global geology of the moon have been hampered by the availability of suitable imaging (≤ 230 m/pix), which covers only 15% of the surface. New data on the abundance of microfeatures (features ≤100 km^2 in area) on a global scale and their locations would help put better constraints on the geophysics of the icy world. We mapped microfeatures in low-resolution images of the E15RegMap01 region of Europa and compared our low-resolution dataset to a validated dataset collected using regional mosaic imaging. We evaluated how many features were missed in low-resolution mapping, the feature types to which they belonged, how often misclassifications were made, and how many false-positive features there were in the low-resolution dataset. We found that microchaos, hybrids, and spots were found at relatively high completeness rates when compared to the regional mosaic dataset, but domes and especially pits were almost always missed. Microchaos, hybrids, and spots also had the highest rates of consistent classification between the low-resolution and regional mosaic datasets. Finally, 36% of our total potential feature count from the low-resolution dataset were revealed to be false positives, mostly caused by ridges and shadows that were mistaken for features in low-resolution imaging. These findings quantitatively estimate the likely errors in existing and future global geologic maps that note the presence of microfeatures, offer remedies to minimize these errors, and provide guidance for future Europa mappers.

1. Introduction

The icy satellite Europa is an important target for astrobiological study, partially because of its known volume of liquid water (Chyba and Phillips, 2007), which could be a present or past habitat for organisms. To accurately assess the potential for life in the solar system, future exploration of Europa should focus on the features most likely to be associated with liquid water. Chaos features are especially compelling targets because of their potential association with heat (Pappalardo et al., 1998; Rathbun et al., 1998; Collins et al., 2000; Sotin et al., 2002; Pappalardo and Barr, 2004; Showman and Han, 2005; Mitri and Showman, 2008; Schmidt et al., 2011), implying they could be linked to liquid water at or near Europa's surface. The study of these features has illustrated Europa's history and helped explain the dynamics of an ice shell over an ocean world.

Large-scale geologic features on Europa's surface have been mapped, particularly large chaos features (Greenberg et al., 1999; Spaun et al., 1998; Prockter et al., 1999; Greeley et al., 2000; Riley et al., 2000; Figueredo et al., 2002; Figueredo and Greeley, 2004; Doggett et al., 2009; Leonard et al., 2019). At smaller scales (≤ 100 km^2 in area), microchaos is found alongside other features of similar size that are also thought to be endogenic, such as domes, pits, and spots, and hybrid features that have characteristics of both domes and microchaos (Greenberg et al., 2003; Singer et al., 2010; Culha and Manga, 2016; Noviello et al., 2019; Singer et al., 2013). These features have previously been called lenticulae in the literature but are here called microfeatures (consistent with Noviello et al., 2019) to emphasize that they are not purely albedo features; examples of each type are shown in Fig. 1. Because small chaos features are co-located with other types of microfeatures and are of similar sizes, many studies (Pappalardo et al., 1998; Rathbun et al., 1998; Collins and Nimmo, 2009; Singer et al., 2010; Schmidt et al., 2011; Michaut and Manga, 2014; Manga and Michaut, 2017; Noviello et al., 2019; Singer et al., 2013) suggest that they share a similar formation process, one likely connected to Europa's heat budget

* Corresponding author.
E-mail address: Jessica.Noviello@ASU.edu (J.L. Noviello).

https://doi.org/10.1016/j.icarus.2021.114495
Received 13 April 2020; Received in revised form 7 April 2021; Accepted 17 April 2021
Available online 23 April 2021

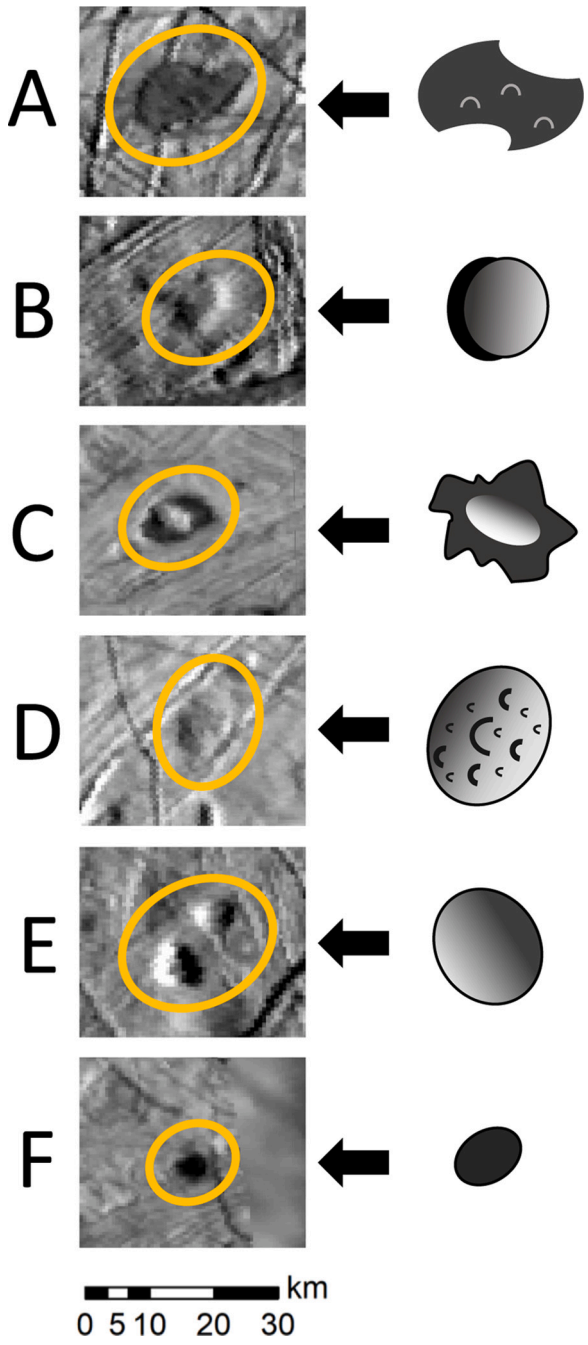

Fig. 1. Examples of microfeatures, identified in regional mosaics of Europa's surface, used here as classification archetypes for the E15LowRes01 mapping dataset. All sun angles from the right. North is up, scale bar is valid for all microfeature types. Microfeatures are to scale in the images. A) Microchaos, classified as such by its irregular shape, the hummocky interior and clear disruption of the previous terrain, and low albedo (though not all microfeatures exhibit low albedos). B) A dome, characterized by its positive topography. C) Type I hybrid morphology, characterized by a positive topographic feature inside of a dark "halo." The halo can be smooth or have a hummocky appearance. D) Type II hybrid morphology, characterized by a positive topographic feature with a fully disrupted surface, akin to the hummocky interior of the chaos feature in 1A. The visible cracks are inconsistent with the surrounding terrain. E) A pit, characterized by its negative topography. F) A spot, characterized by its consistent, low albedo and lack of interior disruption. Adapted from Noviello et al. (2019).

and transport processes within the ice shell.

New data on the abundance of microfeatures on a global scale and their locations on Europa's surface would help put better constraints on the geophysics of the icy world. For example, microfeature formation models predict that chaos and other features would have different global distributions depending on whether they formed via melting (Sotin et al., 2002; Collins and Nimmo, 2009; Soderlund et al., 2014) or via the formation of sills in the ice shell (Schmidt et al., 2011; Michaut and Manga, 2014; Craft et al., 2016; Manga and Michaut, 2017). Determining the locations of additional microfeatures over a larger surface area of Europa than has been previously mapped could identify which of these models is more appropriate for Europa and help direct future modeling efforts.

Most past mapping efforts focused primarily on regional scale-resolution (~230 m/pixel) image mosaics, henceforth called RegMaps (Doggett et al., 2009; Neish et al., 2012; Culha and Manga, 2016; Noviello et al., 2019). RegMaps are good resources for geomorphic mapping on Europa at a finer scale, but only cover ~10% of its total surface area (Doggett et al., 2009). Most of the imaging of Europa's surface falls outside of the regional mosaics at significantly lower resolutions (>1 km/pix). This does not preclude the ability to measure large-scale features (e.g., Leonard et al., 2019), including large chaos features (Neish et al., 2012). Furthermore, Leonard et al. (2019) have produced global geologic maps of Europa that included potential microchaos features within low-resolution images. These maps did not differentiate between potential microchaos and other microfeatures.

The results of mapping studies, especially those that focus on chaos features, are also greatly affected by the imaging parameters. In general, when mapping with high-resolution images and higher incidence angles, the successful (and consistent) identification of chaos regions increases (Riley et al., 2000; Hoppa et al., 2001; Neish et al., 2012). These studies focused on finding and identifying large ($\geq$ 1500 km^2 in area) chaos features, far larger than the size cut-off for microfeatures, including microchaos ($\leq$ 100 km^2). Additionally, the success rates of mapping and identifying non-chaos microfeatures in low-resolution imaging have not been quantified.

Low-resolution *Galileo* imaging contains a wealth of potentially usable data that has not yet been fully explored. If additional morphologic data could be gleaned from this dataset, we could better constrain models for microfeature formation. Here we find and describe the limits of microfeature identification in low-resolution images by creating a dataset of features in low-resolution images and comparing it to a published dataset collected in the same area using the E15RegMap01 mosaic (Noviello et al., 2019). Directly comparing these datasets will help determine the main sources of error and quantify uncertainty when mapping microfeatures in low-resolution images. Here, we specifically look for microfeatures in an area covered by both regional-mapping and low-resolution imaging to quantify the error rates in both omitting and misclassifying features. These results can lead to a stronger interpretation of existing global maps that noted microchaos (Leonard et al., 2019), but did not differentiate it from other microfeatures on Europa, in order to refine microfeature formation models. These constraints could also be applied to future efforts to map microfeatures outside of traditional regional mosaics to provide additional constraints for microfeature formation and heat and material transfer models. In turn, these maps can enhance our understanding of Europa's geology ahead of the flagship Europa Clipper mission (Phillips and Pappalardo, 2014; Pappalardo et al., 2016; Pappalardo et al., 2017), strengthen the justification for certain scientific objectives, and increase the success of the overall mission.

2. Methods

2.1. Images used

One region, E15RegMap01, was selected as a low-resolution

mapping test case. Only images taken with the *Galileo* SSI (Belton et al., 1992) broadband clear filter (central wavelength 611 nm) were included. Details of these images are included in the Supplementary Material, along with a description of the photometric correction applied to them using the USGS ISIS3 software (Torson and Becker, 1997; Anderson et al., 2004); for a full description of this region, see Noviello et al. (2019). The E15RegMap01 images had average resolutions ranging from 228 to 234 m/pixel. We used the USGS Planetary Image Locator Tool (PILOT; USGS, 2020) to identify appropriate images that covered the E15RegMap01 area. We constrained our search to images with resolutions between 1.4 and 1.7 km/pixel (at least six times the resolution of the E15RegMap01 images) and images taken with the clear filter to eliminate any bias in using another filter. In total, five images met these criteria, and four images that collectively covered the full study area were used for the low-resolution mapping. The fifth image covered a redundant area to one of the other images and was therefore not considered. The area studied in this work is the same as that in the G1ESGLOBAL01 mosaic; however, because we evaluate the four images independently and because we only study the part of the region that is also covered by the E15RegMap01, we distinguish it by a different name, E15LowRes01.

These images were processed using the USGS ISIS3 software (Torson and Becker, 1997; Anderson et al., 2004), positioned using the established Europa basemap (USGS, 2002), and examined individually. Details of the four low-resolution images are provided in Table 1 for only the parts of the images used in the low-resolution mapping, and Table 2 for the average values across the entire image. The incidence angle range for areas mapped within these images spans 37.43–57.30°. These are relatively low incidence angles for identifying microchaos according to Neish et al. (2012), who recommended incidence angles >70°; this is discussed extensively in Section 4.3. Maps showing the E15RegMap01 study area and the low-resolution images' overlap with E15RegMap01 are provided in Fig. 2.

2.2. Dataset collection

To assess completeness and accuracy, the low-resolution dataset collected in the E15RegMap01 area (here called E15LowRes01) was directly compared to the E15RegMap01 dataset described in Noviello et al. (2019) and whose microfeature attributes are summarized in the first line of Table 3. The E15RegMap01 dataset was collected using the individual images detailed in the Supplementary Material, and compiled from and validated against four independently collected datasets (Greenberg et al., 2003; Singer et al., 2010; Culha and Manga, 2016; Noviello et al., 2019; Singer et al., 2013) to ensure the most accurate and robust microfeature dataset.

The low-resolution data were mapped using the same methodology employed to collect the four RegMap datasets described in Noviello et al. (2019). The boundaries of potential features were mapped as polygons in ArcGIS. Using ArcGIS tools, we collected information about each feature's mapped area, perimeter, latitude, longitude, maximum length, and maximum width. In addition to area and perimeter, we also calculated the equal area diameter for each feature, defined as the diameter of a circle that has the equivalent area as the feature. We used this value to estimate the minimum size of a visible feature using the reasonable lower limit of five pixels (e.g., Singer et al., 2013), and determined that 7.5 km is the expected minimum diameter of a visible feature in the E15LowRes01 dataset.

We chose five pixels for two reasons, the first being that five pixels should help minimize the erroneous mapping of false positives, and the second being the size restrictions of the microfeatures themselves. While some previous studies suggest a typical microfeature size around 10 km in diameter (Carr, 1998; Greeley et al., 2000; Pappalardo et al., 1998; Spaun et al., 1999), other work (Greenberg et al., 2003; Noviello et al., 2019) has not found evidence to support that except perhaps in the case of microchaos, as noted first in Pappalardo et al. (1998) but questioned in Riley et al. (2000). All other microfeature types have average maximum lengths that range between 4 and 9 km, with pits, domes, and spots peaking in the 5–8 km range and hybrids and microchaos in the upper range. In terms of their equal-area diameters (the diameter of a circle with an equivalent area), the peaks are between 4 and 5 km, even smaller sizes than the maximum length. Five pixels in the low-resolution images corresponds to the 7.5 km expected minimum diameter mentioned previously. Therefore, we expect our dataset to favor the larger microfeatures of all categories, particularly microchaos and hybrids, though we did not actively avoid mapping microfeatures under this limit.

The microfeatures were then classified into one of the defined microfeature groups based on their appearance in the low-resolution images. The morphology types are as follows: microchaos, a relatively flat feature that has clear disruption of its interior; domes, features with positive topography as determined by the direction of shadows; pits, features with negative topography as determined by the direction of shadows; spots, features of no apparent topography and near-uniform low albedo; and hybrids, features that have a mixture of microchaos features (irregular shapes, disrupted interiors, etc.) and domes. These feature types are shown in Fig. 1. Ambiguous microfeatures were assigned to the "unclassified" group.

We note that, because the same person did the mapping for both the regional mosaic map and the low-resolution image map, a previous knowledge of the area may have influenced the low-resolution classifications at some level. However, there was a gap in time of about 10 months between data collection and the regional mapping project encompassed four different regions of Europa, likely reducing the biasing effect of prior knowledge within this one region. Still, this is a source of bias in the datasets, and therefore the accuracy values (discussed in the next section) presented here should be considered to be upper limits.

2.3. Completeness and accuracy rates

To better assess the completeness of the E15LowRes01 dataset, we report the "find rate," which is defined as the percentage of features mapped in E15RegMap01 that were also identified in E15LowRes01, even if the classification of the feature was inconsistent between the two. The find rates for all categories are given in the last row of Table 3. Once features are found in E15LowRes01 imaging, the next step is to determine how often the classifications done in the E15LowRes01 dataset are consistent with the E15RegMap01 classifications, which are assumed to be more robust. This is done by comparing the classification made in

Table 1
The imaging characteristics of the low-resolution *Galileo* images used for mapping in this study, including the unique identifier of the spacecraft clock start count number (s_clocknumber). These details represent the range of imaging parameters across only the part of the image used for mapping except for the column that specifically says "Whole Image" (see Fig. 2 for a visual representation of this).

Image ID (s_clocknumber)	Orbit Acquired On	Incidence Angle Range (°)	Emission Angle Range (°)	Phase Angle Range (°)	Pixel Resolution Range in m/px
5139r (03498751.39)	G1	40.30–41.29	2.98–20.48	37.51–37.55	1570.42–1571.40
5126r (03498751.26)	G1	37.43–52.25	17.38–19.27	34.03–37.40	1571.11–1571.26
5113r (03498751.13)	G1	42.25–54.45	6.62–27.09	37.40–37.47	1570.47–1572.10
5100r (03498751.00)	G1	51.58–57.30	15.02–35.99	37.37–37.41	1570.88–1573.37

Table 2
The average imaging characteristics of the low-resolution *Galileo* images including the unique identifier of the spacecraft clock start count number (s_clocknumber). The average incidence angles of these images do not accurately represent the values of the area studied (Table 1), emphasizing the need to use the parts of low-resolution *Galileo* imaging most suited for regional mapping (e.g., those with moderate-to-high incidence angles following Neish et al., 2012).

Image ID (s_clocknumber)	Galileo Orbit Acquired On	Average Phase Angle	Average Emission Angle	Average Incidence Angle	Incidence Angle Range (°)	Average Pixel Resolution in m/px
5139r (03498751.39)	G1	37.72	32.36	30.29	2.1416–69.86	1572.85
5126r (03498751.26)	G1	37.72	24.15	21.14	0.02–54.31	1571.76
5113r (03498751.13)	G1	37.30	27.41	61.65	36.73–116.92	1572.13
5100r (03498751.00)	G1	37.25	35.43	67.68	38.39–120.74	1573.27

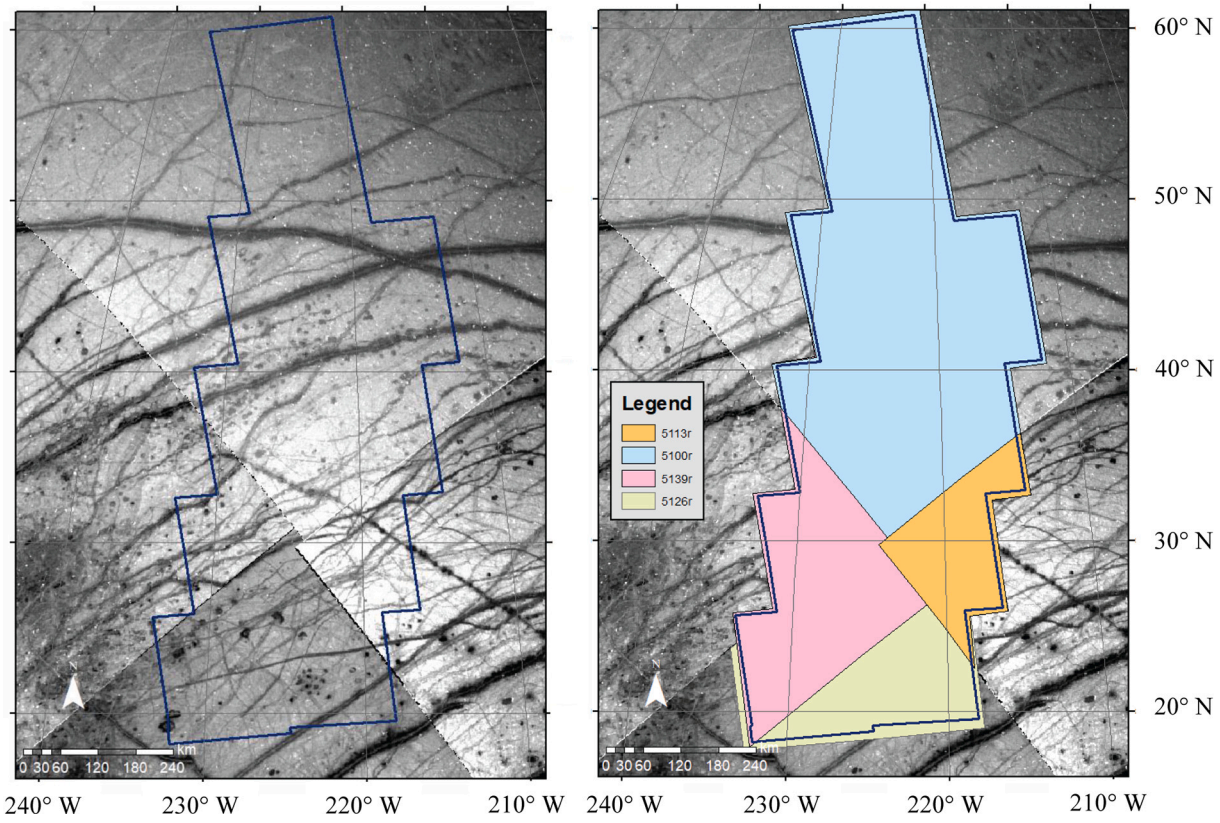

Fig. 2. A) The E15RegMap study area (with navy blue outline) with the low-resolution images overlain. No single image covered the entire study area, hence why four total images were used. Details about these images are provided in Table A1. B) The E15RegMap study area (navy blue outline) with low-resolution imaging coverage polygons overlain. This represents which parts of E15RegMap01 were mapped in which image. These images used here are 5100r (s_clocknumber = 03498751.00), 5113r (s_clocknumber = 03498751.13), 5126r (s_clocknumber = 03498751.26), and 5139r (s_clocknumber = 03498751.39). (For interpretation of the references to color in this figure legend, the reader is referred to the web version of this article.)

Table 3
Count breakdown of all microfeatures mapped in E15LowRes01 compared to the higher-resolution dataset, E15RegMap01. The total number of features mapped in E15RegMap01 is 339, the total number of features mapped in E15LowRes01 is 214, and the total number of missed features is 195. Only microfeatures ($\leq$100 km^2 in area) are reported in this table.

Data Set	Total	Chaos (%)	Domes (%)	Hybrids (%)	Pits (%)	Spots (%)	Unclassified (%)
All E15RegMap01 microfeatures	310	68 (21.9)	33 (10.6)	36 (11.6)	119 (38.4%)	23 (7.4%)	31 (10.0)
E15LowRes01 microfeatures (classified in low-resolution images)	187	83 (44.4)	11 (5.9)	6 (3.2)	6 (3.2)	53 (28.3)	28 (15.0)
Missed E15RegMap01 microfeatures	193	15 (7.8)	25 (13.0)	12 (6.2)	113 (58.5)	6 (3.1)	22 (11.4)
Find rate	x	77.9%	24.2%	66.7%	5.0%	73.9%	29.0%

both datasets and noting if they match. If they match, then it is counted as a successful identification. We also quantify the rates of false positives by studying the "phantom" feature rate, or the amount of times a potential feature was mapped in the low-resolution dataset but was revealed to have no corresponding feature of any type in the higher-resolution E15RegMap01 dataset.

3. Results

3.1. E15LowRes01 mapping and identification

In total, 214 total features were mapped in E15LowRes01; this map is shown in Fig. 3A. The equivalent diameter of all of these features ranged from 2.33 km to 21.25 km. The minimum equivalent diameter of

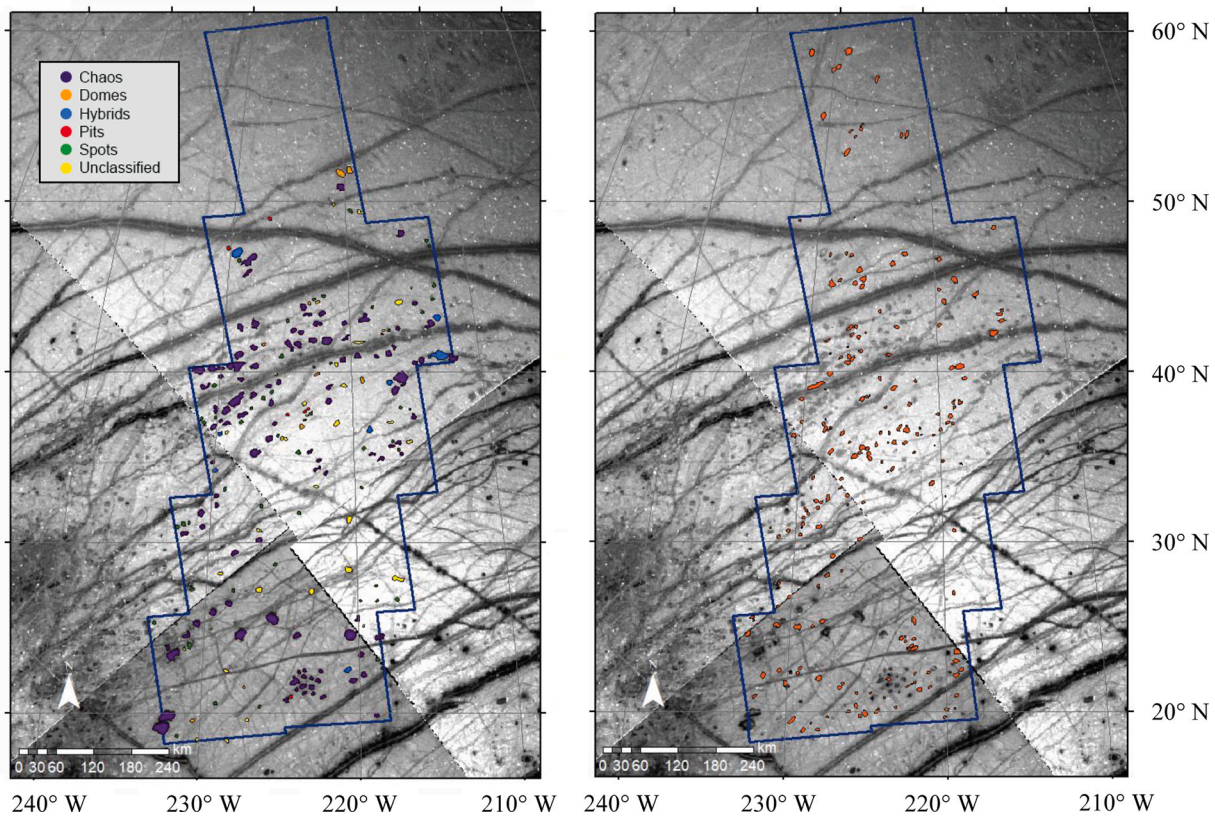

Fig. 3. A) Map showing all features mapped in the E15LowRes01 dataset, including phantom features that have no corresponding feature in the regional mapping data set. Classifications here refer to the low-resolution classification. The features whose boundaries extend outside of the map limits were excluded from the dataset prior to analysis, as well as any features whose area was above 100 km^2. B) All features (in orange) of the E15RegMap01 study area missed in low-resolution mapping of the same area. The navy blue outline represents the extent of the study area. (For interpretation of the references to color in this figure legend, the reader is referred to the web version of this article.)

mapped features in the E15LowRes01 dataset is less than the estimated minimum size using the "five pixel rule," mainly due to albedo differences that made them more obvious (see Discussion). Based on the size limit within the definition of microfeatures (equivalent diameter $\leq$ 11.28 km), 187 of the mapped features are considered microfeatures; their type breakdowns are provided in Table 3. Of these 187 presumed microfeatures, 70 (37.6%) of the features mapped have equivalent diameters above 7.5 km, the assumed minimum size for features that would be visible in the low-resolution imaging. These 70 features were classified in low-resolution imaging as: 55 microchaos (78.6%), two domes (2.9%), four hybrids (5.7%), no pits, two spots (2.9%), and seven unclassified features (10.0%).

3.2. Missed features and find rates

Features were considered "found" if a feature in the E15LowRes01 dataset overlapped with a feature in the E15RegMap01 dataset. Out of the 310 features identified in the higher resolution E15RegMap01 dataset, a total of 195 features were not mapped at all in E15LowRes01 and are considered missed (Fig. 3B). Out of these 195 missed features, 193 are within the microfeature size cut-off ($\leq$ 100 km^2 in area or under 11.28 km in equivalent diameter), and nearly all (187, 96.9%) are above 2.5 km in equal-area diameter, almost the smallest size mapped in the E15LowRes01dataset. Hence, we consider 187 of these features as "findable" based solely on their size. The distribution of the diameters of the missed features has a peak between 5 and 6 km (Fig. 4A and B) and qualitatively matches with the distribution of the microfeatures mapped in E15LowRes01, suggestive of minimal size bias between missed and mapped features. The measured find rates for features by bin size (Fig. 4C) is also relatively constant except for at small and at large microfeature sizes, again suggestive of minimal size bias.

The measured sizes of the microfeatures between the two datasets is also of interest, as it might be expected that the microfeatures mapped in the low-resolution imaging would have a larger average size their corresponding microfeatures mapping in the regional mapping imaging size due to the coarser resolution. To evaluate this, we compared the equal area diameters of only the features that had been found as measured in both datasets. We define the equal area diameter to be the diameter of a circle with equal area to the feature and calculated with the equation $Diam. = 2*\sqrt{\frac{Area}{\pi}}$. Microchaos, domes, hybrids, and spots mapped in low-resolution were larger on average than their regional mapping counterparts. Microchaos, domes, and hybrids mapped in low-resolution all had a less than 10% size increase compared to the regional mapping dataset (3.6%, 9.8%, and 8.5%, respectively). Spots in low-resolution were 23.4% larger, on average, than their counterparts in the regional mapping. Pits were the only features that were mapped to be smaller on average in the low-resolution dataset than in the regional mapping one (smaller by 19.9%). We discuss some reasons for this in the Discussion section.

The type breakdowns of the missed features are also given in Table 3. Pits are noticeably rare in the E15LowRes01 data set despite having been the most numerous microfeature type (by nearly a factor of two) in the regional mapping data set. In several cases, we report more features of a given type within the low resolution data set than were found in the high resolution data set, which is caused by both misclassification (see next section) and false positives. Features mapped in the E15LowRes01 dataset that did not have a corresponding microfeature in the E15RegMap01 dataset are the false positives, which we refer to as phantom features. In total there were 76 phantom features, of which 68

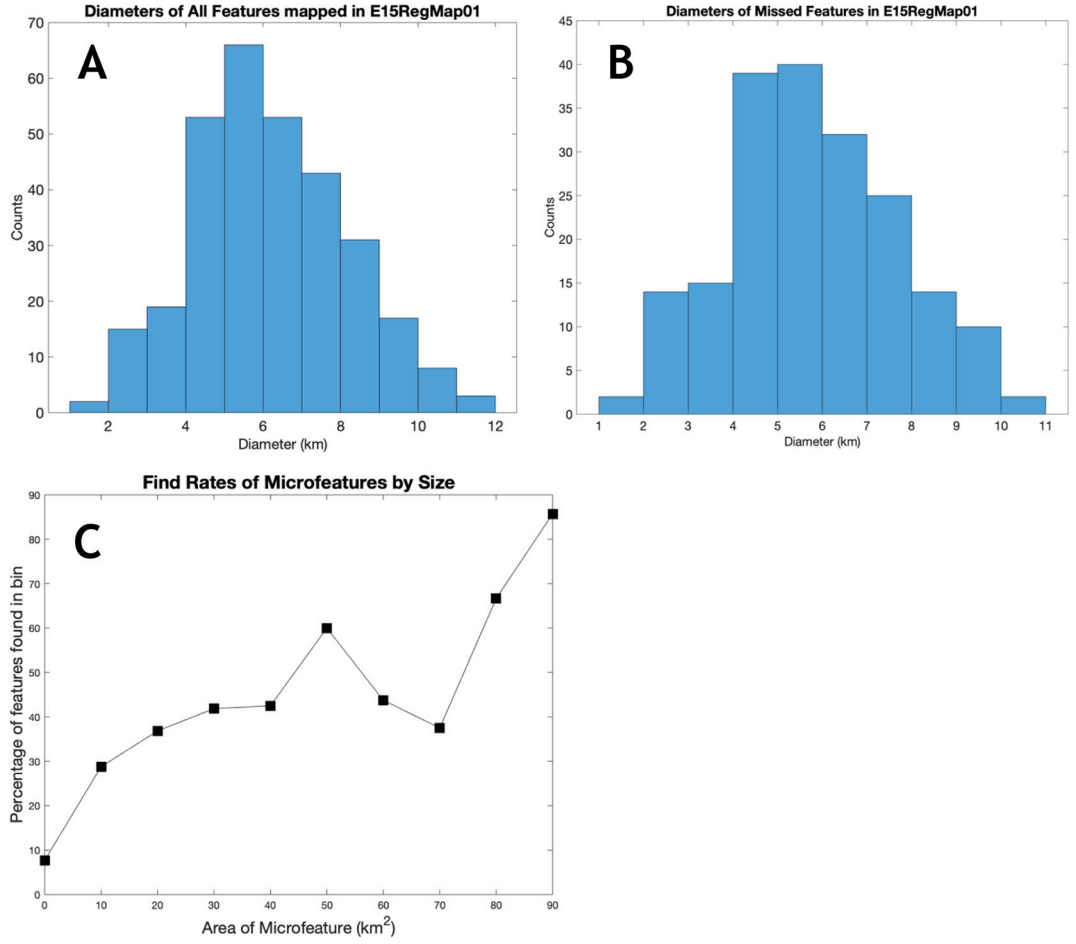

Fig. 4. A) Histogram of equal-area circle diameters for all microfeatures successfully mapped in the original E15RegMap01 dataset; B) All missed microfeatures from the E15RegMap01 dataset. C) The find rates for microfeatures in E15RegMap01 as a function of their areas. Bin sizes for diameters are fixed at 1 km for both A and B. For C, they are fixed at 10 km^2.

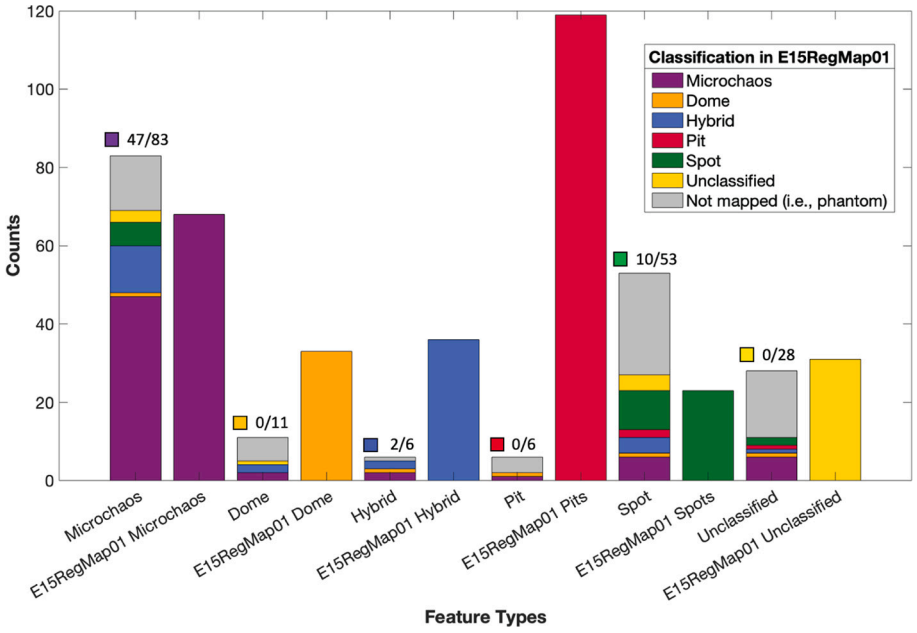

Fig. 5. A stacked bar histogram showing the count of features mapped in the E15LowRes01 dataset that were classified correctly, misclassified, or unmapped features (i.e., the phantom features). The solid bars represent the total number of that microfeature type mapped in the E15RegMap01 dataset. The numbers above the bars show the total number of features that were mapped and correctly classified compared to the total number of features mapped for that feature type in the E15LowRes01 dataset. The colors in the small boxes above the bars represent the color of the correct feature type for that bar.

were under the microfeature size cut-off.

3.3. Accuracy rates

Accuracy in this context is the ability to find a feature in both low-resolution and the E15RegMap01 imaging and have a consistent classification of that feature between both datasets. When comparing the classification of a feature in lower resolution with that made using the higher resolution images, we found that some microfeatures groups were mapped more accurately than others (Fig. 5). Microchaos features were correctly classified 47 out of the 83 times (56.6%) they were mapped, domes were correct zero out of 11 times, hybrids were correct two out of six times (33.3%), pits were correct zero out of six times, and spots were correct ten out of 53 times (18.9%). The classification accuracies for each microfeature type are in the boxes highlighted in green in Table 4. Also included are the occasions where phantom features were detected and mapped and the category to which they were assigned in the E15LowRes01 dataset. The general accuracy rates (Table 4 and Fig. 5) of mapping depend on whether or not the unclassified features are included in the calculation. In total there were 28 unclassified features in the E15LowRes01 dataset. However, there were no features assigned to the "unclassified" group in the E15LowRes01 dataset that were also unclassified in the E15RegMap01 dataset (Table 4). The overall accuracy rate of our low resolution mapping is 59 out of 187 (31.6%) when E15RegMap01 unclassified features are included, and 59 out of 159 (37.1%) when they are excluded.

4. Discussion

The microfeatures initially mapped in the E15RegMap01 region, including those left unclassified, number 310. A total of 193 of these microfeatures were not identified in the E15LowRes01 data set. This implies that 117 microfeatures were found, a number verified by looking at the dataset directly. If there are 187 microfeatures mapped and 68 of them are false positives, that should mean that 119 features mapped in the E15LowRes dataset correspond to a real feature in the E15RegMap01 dataset. This apparent discrepancy in the numbers is remedied when examining the datasets more closely. Some of the low-resolution microfeatures are large enough to touch two features in the E15RegMap dataset, mistakenly marking two features as "found." This happened five times in this analysis, but only resulted in two extra features counted as "found" that would not have been counted otherwise. Overall this suggests that a low percentage (five out of 187, 2.7%) of features could truly be multiple, closely-spaced individual features whose boundaries cannot be distinguished in low-resolution imaging. An example of this kind of error is shown in Fig. 6.

We also consider the reason for the found microfeature size differences between the low-resolution and regional mapping datasets. For microchaos, domes, and hybrids, the size differences were all less than 10%. This suggests that these features are being mapped as roughly true to size, especially for the microchaos. It is likely that the albedo difference of microchaos against Europa's background lends itself well to accurate size mapping. Not all hybrid features have a low albedo (e.g., Type I hybrids), which could explain why hybrid features have a size increase more similar to domes than to microchaos. For spots, the size difference between the datasets was 23.4%, significantly larger than for microchaos, domes, or hybrids. The likeliest source of this increase is related to the fact that spots are the smallest of all of the microfeatures (Noviello et al., 2019). Any spots that were successfully mapped were

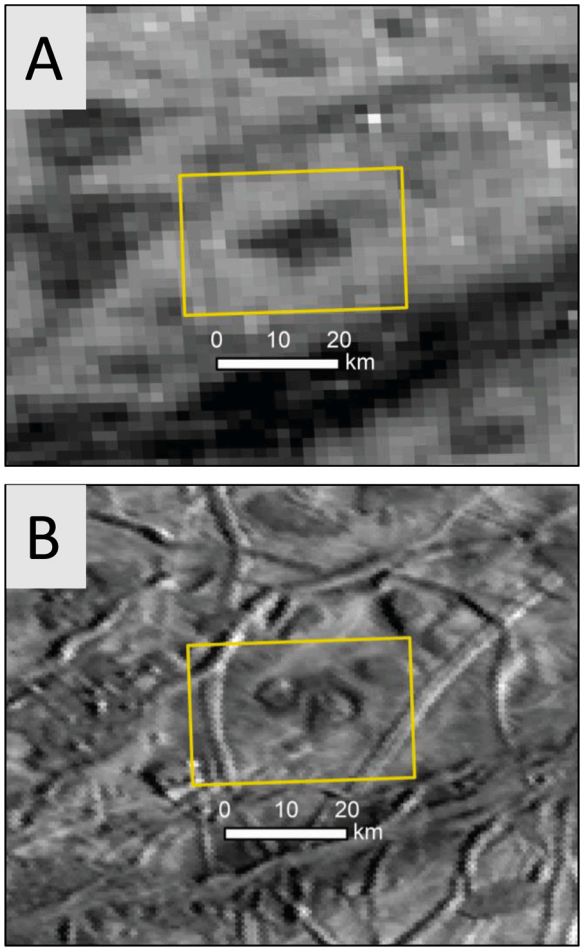

Fig. 6. An example of a case where a presumed single feature mapped in a low-resolution image (A) is revealed to be two separate features in the regional-scale imaging (B). In this case, the feature was classified as a single chaos feature in the low-resolution dataset but was classified as two separate hybrid features in the E15RegMap01 dataset. Thus, this is both a case of two microfeatures merging into one in low-resolution imaging and misclassification. This error is uncommon; only 2.7% of all potential microfeatures mapped in low-resolution imaging were revealed to be two separate features.

Table 4
Classification accuracy breakdown of all microfeatures mapped in E15LowRes01. The columns across represent the classifications in the E15RegMap01 dataset, and the rows down represent the classifications made in the E15LowRes01 dataset. The values highlighted in green are the ones whose classifications matched between the two datasets.

	Total	Microchaos Counts (%)	Dome Counts (%)	Hybrid Counts (%)	Pit Counts (%)	Spot Counts (%)	Unclassi-fied Counts (%)	Phantom Counts (%)
Micro-chaos	83	47 (56.6%)	1 (1.2%)	12 (14.5%)	0	6 (7.2%)	3 (3.6%)	14 (16.9%)
Dome	11	2 (18.2%)	0	2 (18.2%)	0	0	1 (9.1%)	6 (54.5%)
Hybrid	6	2 (33.3%)	1 (16.7%)	2 (33.3%)	0	0	0	1 (16.7%)
Pit	6	1 (16.7%)	1 (16.7%)	0	0	0	0	4 (66.6%)
Spot	53	6 (11.3%)	1 (1.9%)	4 (7.5%)	2 (3.8%)	10 (18.9%)	4 (7.5%)	26 (49.1%)
Unclassi-fied	28	6 (21.4%)	1 (3.6%)	1 (3.6%)	1 (3.6%)	2 (7.1%)	0	17 (60.7%)
Phantom	68	14 (20.6%)	6 (8.8%)	1 (1.5%)	4 (5.9%)	26 (38.2%)	17 (25.0%)	x

likely to be larger by default, and thus the increase in average size would be more severe. Indeed, many spots were large enough to be mistaken for chaos in low-resolution imaging (Table 4). Pits were the only feature that had a smaller size in the low-resolution mapping than in the regional mapping (~20% smaller); however, this number is almost certainly incorrect, as there are only three pits in the "found" dataset, not nearly enough to draw robust conclusions. This means that efforts to map microchaos, domes, and hybrid features can consider the low-resolution features roughly accurate in size, if slightly too large, but spots and pits should be approached with more caution.

4.1. Effects of size of microfeatures on mapping in low-resolution imaging

There does not appear to be a clear size cut-off below which a majority of features are missed, though we do note from that by using the 7.5 km (five pixel) size cut-off, we would exclude smaller features such as the pits, domes, and spots by default. If it was difficult to identify microfeatures below a certain diameter size, the histogram of missed microfeatures would show a plateau in the histogram up to that size, and above that the missed counts would decrease, signaling few missed microfeatures. This is not observed, nor is it observed in the find rates when compared to microfeature areas (Fig. 4C). The smallest confirmed feature identified in the low resolution images was a spot that was 3.56 km in equal-area diameter. This feature also had a consistent classification between the E15LowRes01 and E15LowRes01 datasets as a spot. As the smallest feature type, spots were also at a disadvantage for being found, but were overrepresented in the low-resolution dataset largely because of their low albedo contrasting with high albedo plains material on Europa (though many of these "spots" were revealed to be false positives). The smallest feature mapped in this dataset was 2.33 km in equal-area diameter (put in the "unclassified" group), well below the five-pixel detection limit of 7.5 km, but this feature was revealed to be a phantom feature. Overall, this work shows that it is possible to map microfeatures on Europa as small as 2.5 km in diameter even in low-resolution imaging in some cases, though the accuracy of these classifications is very low.

Rather than a 7.5 km (five pixel) limit, a more appropriate rule for detecting features on a bright surface such as Europa could be as small as 2.5 km in diameter if the feature has an apparent albedo that differs significantly from the background, as many of the microchaos, hybrid, and spot features do, but the likelihood of these potential features being true features is low. The phantom feature rate drops to under 50% when features are larger than 20 km^2 in area (~5.0 km in equal-area diameter), and drops to about 25% above this size. Therefore, the smallest size feature that can be mapped and classified with a moderate level of confidence is around 5.0 km in diameter. To maximize information out of future datasets, we recommend that future low-resolution mapping efforts of Europa actively map and classify features as small as 5 km in diameter. Smaller features can be mapped but must be interpreted cautiously, as they are highly likely to be phantom features.

Another finding regarding microfeature size is that the accuracy rate for microfeatures increases as size increases from 10 to 100 km^2. A simple linear model (y-intercept = 11.494, 95% CI:[−1.46, 24.45], *p*-value = 0.075; slope = 0.646, 95% CI:[0.40, 0.89], p-value <0.001) yields a high positive correlation ($r_{sq} = 0.825$, $r_{sq.,\ adj.} = 0.803$) between accuracy and size (Fig. 7A), though much of the accuracy at larger sizes is dominated by microchaos (Fig. 7B). The correlation coefficient means that the linear model can explain about 80% of the variation observed in the data. The general positive trend makes sense, as a larger feature should be easier to identify because its details should be more apparent. Small-sample statistics may be the reason that at smaller sizes the accuracy rate is higher than predicted by the model, and actually drops initially as sizes of the features increase. It may be that the smallest microfeatures were only found because their apparent albedos contrasted with the surrounding terrain, which made them both visible and more likely to belong to the microchaos, hybrid, or spot classifications.

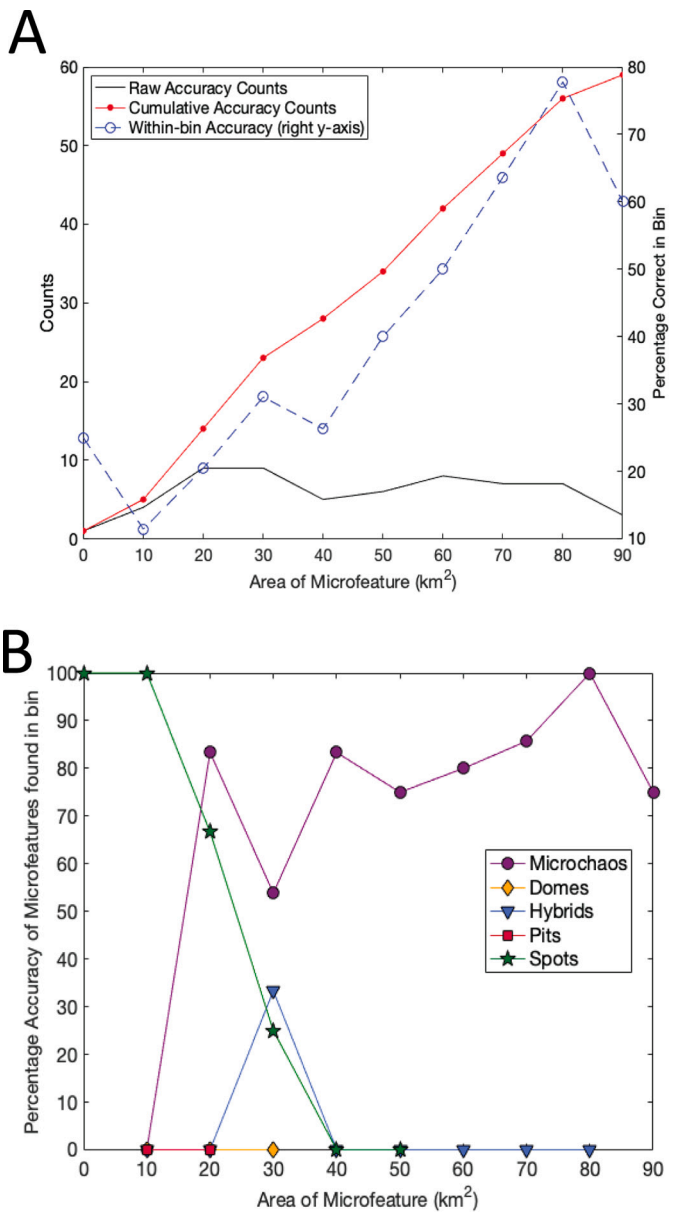

Fig. 7. A) Accuracy of E15LowRes01 classification as a function of size, shown as a line histogram. Solid lines follow the left y-axis, dashed lines follow the right. The bins represent 10 km^2 in area and are plotted at the left edge of the bin (e.g., the measurements for the 20–30 km^2 bin are plotted on the 20 km^2 line). Accuracy is defined as when a feature mapped and classified in E15LowRes01 is mapped in the same place as another feature with the same classification in the regional mapping dataset. The black line represents the raw counts per bin (number of correct cross-classifications), and the red dotted line represents the cumulative number of correct classifications for all the bins. The blue dashed line with open circles represents the percentage of correct classifications per bin relative to the total number of features per bin. The blue line follows the scale on the right y-axis. The trend is that as microfeature size increases, the number of correct classifications (accuracy) also increases. The linear regression of accuracy versus area yields a slope of 0.646, a y-intercept of 11.494, and an r^2_{adj} of 0.803. B) The breakdown of the accuracy of these features as a function of size and microfeature type. High accuracy rates at large sizes are largely driven by microchaos, which is both relatively easy to map in low-resolution imaging and the largest microfeature type. (For interpretation of the references to color in this figure legend, the reader is referred to the web version of this article.)

Simultaneously, the larger microfeatures that had apparent albedos similar to the terrain did not provide enough visual information to make an accurate classification.

One additional yet important detail of this result is that microchaos tends to dominate the overall counts at larger sizes, making a person more likely to call a larger feature microchaos, especially if it also has a low relative albedo. Hybrid features also are larger on average than pits, domes, and spots, though to a lesser extent than microchaos (Noviello et al., 2019). This is represented in Fig. 7B, which shows that microchaos classifications tend to drive the higher accuracy rates. Prior knowledge of these facts could lead to a larger feature being called microchaos by default, unless it is clear that the feature fits better in another group. Microchaos, hybrids, and spots also tend to have a lower albedo than the surrounding terrain, making them more visible than equally-sized domes and pits, though apparent albedo is also highly dependent on imaging angles (Hoppa et al., 2001; Neish et al., 2012). We stress that the ability to find a relatively large feature area and/or a darker patch on Europa's surface is not a guarantee of correct classification, but they are helpful pieces of information.

4.2. Find and accuracy rates

The accuracies of our classifications are shown graphically in Fig. 5, in which the x-axis denotes the classifications made in either low-resolution or the E15RegMap01 dataset. The stacked bars then break down the number of classified features into their designations within the regional mapping data set using the colors listed in the legend. We also provide the number of microfeatures of that type that were mapped in the E15RegMap01 dataset as solid-colored bars next to the multicolored ones. Because the same person mapped both the regional mosaic and the low-resolution datasets, the low-resolution dataset collection was at least partially influenced by prior knowledge of the region. Thus, these numbers should be considered an upper limit on accuracy rates.

The overall accuracy of correctly classified microfeatures is 59 out of 187, or 31.6%. Microchaos, hybrids, and spots were found at relatively high rates (66.7 to 77.9%), even though these were often misclassified. Domes and pits were found at very low rates, only 24.2% and 5.0% of the features mapped in higher resolutions, respectively, and the accuracy of features classified as pits and domes in low resolution was zero. The hybrid features that were not mapped in the low-resolution dataset (an error of accidental omission) all belonged to the Type II (cracked dome) subcategory described in Noviello et al. (2019), as opposed to the Type I hybrid subcategory, which look like a low-albedo dome surrounded by a hummocky moat reminiscent of some chaotic terrain. That Type II hybrid features are missed more often than Type I is consistent with the finding that domes are missed more often than microchaos features, and that low albedo features are easier to identify. Fig. 8 shows an example of a Type II hybrid feature that was accidentally omitted in the low-resolution mapping.

Importantly, not all low-albedo features mapped in low-resolution images can be correctly interpreted to be microchaos or chaos-related features; roughly 40% of all features that were called "chaos" in the E15LowRes01 dataset were revealed to be misclassified microfeatures or phantom features in the E15RegMap01 dataset. An argument can be made that microchaos, spots, and hybrid microfeatures are inherently related due to their similar characteristics, particularly their low apparent albedos (Prockter et al., 1999; Greeley et al., 2000; Neish et al., 2012; Leonard et al., 2019; Noviello et al., 2019) and association with salt (Hand and Carlson, 2015). If chaos-related microfeatures are considered chaos-related features in E15RegMap01 and other RegMap areas, then the microchaos accuracy rate increases to 59 out of 83 times, or 71.1%. In other words, if a feature is mapped and classified as microchaos, it has a roughly 70% chance of being either a microchaos, hybrid, or spot. However, if we try to combine our classifications of microchaos, hybrids, and spots, our misclassifications of hybrids and spots reduces the overall correct percentage to 41.5% (59 out of 142 total). We thus conclude that low-albedo microfeatures are more likely to be identified, but not more likely to be correctly classified.

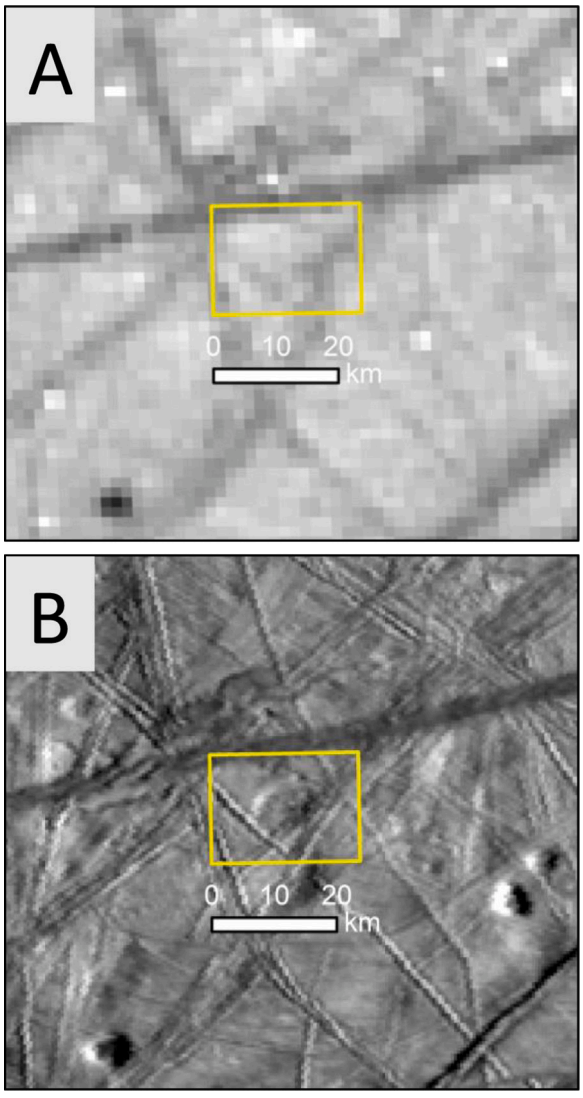

Fig. 8. An example of an accidentally omitted ("missed") Type II hybrid microfeature. A) It is not distinguishable in low-resolution imaging, but, as shown in B) its topography and morphology are clearly visible in the regional mosaic imaging, very likely due to the higher incidence angle in the regional imaging. Other examples of "invisible" features in the low-resolution imaging are seen to the east of the highlighted feature. One dark feature to the southwest of the highlighted feature was mistakenly classified as a spot in the low-resolution dataset, when the regional-scale imaging reveals it to be a shadow. North is up.

Hybrids and spots are found at higher rates than domes and pits, but their identification accuracy rates are still relatively low (Figs. 5 and 7B). Hybrids were found at a rate of 66.7% but accurately classified as hybrid features only twice out of six times. Instead, hybrid features were incorrectly classified as microchaos features, domes, or an unmapped area. Spots were fairly easy to find in the E15LowRes01 imaging (find rate = 73.9%), but roughly half of the "spots" identified in E15LowRes01 were phantom features (49.1%). Additionally, at least one spot was misclassified into every potential microfeature group, though the most common incorrect category aside from phantom was microchaos (11.3%).

4.3. Missed features and the effects of imaging parameters on low-resolution mapping

A total of 15 microchaos features were missed, and we examined these features more closely to determine why. Two of these microchaos features were associated with an anomalously bright spot in the E15LowRes01 imaging; these bright spots corresponded to the illumination of a topographic high nearby, and the microchaos' shape and relatively low normalized albedo was lost. Two more microchaos features were too close to ridges and did not appear as a separate feature in the images, so they were not mapped. Four of the missed microchaos features were indistinguishable from the background terrain in the E15LowRes01 imaging. The remaining nine microchaos features had no discernable reason for why they were missed and were simply omitted during the low-resolution mapping. We examine some potential reasons for this here.

The reason for these errors of omission are likely due to the variation in imaging parameters between the E15RegMap01 and the E15LowRes01 images. In the E15RegMap01 images, the incidence angles range between 73.75 and 80.84°, while in the low-resolution images, the range was 37.43–57.30°, a wider range and a lower overall value than in the E15RegMap01 images. At these low incidence angles, the images emphasize the albedo characteristics of these microfeatures over those of morphology or topography. According to Hoppa et al. (2001), smoother modified chaos (as opposed to fresh chaos following the definitions of Greenberg et al., 1999) is more apparent in images with an incidence angle range between 71 and 78° because the higher incidence angles highlight morphology (individual chaos rafts and/or lineaments within the matrix). We do not seek here to detail the morphology of the microchaos we map, only to quantify its presence in two datasets, but we still must consider the effects that imaging parameters had on finding the microfeatures at all.

To study the effects of observational parameters on chaos identification, Neish et al. (2012) mapped chaos regions in regional mosaics, regional mosaic images that had been artificially degraded to the resolution of a low-resolution image, and images originally taken at low-resolutions. In cases when the resolution was low (~1.5 km/pix) but the incidence angle was high (≥70°), large chaos was easily identified. In images with low incidence angles (≤30°), however, chaos could not be identified even if the resolution was 250 m/pix or less (Neish et al., 2012). The incidence angles of the low-resolution images used in this study are above 30°, but not by much, so it is likely that the incidence angle is responsible for many of these omissions. Though we've shown that this low-resolution dataset is not complete, corroborating previous results (Prockter et al., 1999; (Hoppa et al., 2001) Neish et al., 2012), it is not that far off in terms of total number of microchaos features mapped in the low-resolution images. Both the find and accuracy rates for microchaos were the highest out of all the microfeature types, at 77.9% and 56.6%, respectively. This may be a reflection of the microchaos themselves, as they presented with particularly low albedos. Because features generally tend to brighten with age on Europa (Pappalardo and Sullivan, 1996; Geissler et al., 1998; Prockter et al., 1999; Fanale et al., 2000; Prockter et al., 2017), the darker microchaos features mapped in the low-resolution dataset are probably relatively young.

A separate question is whether microchaos is more accurately identified in images with higher incidence angles, which would be consistent with the findings of Neish et al. (2012). Given the constraints on these images in this region, we cannot fully verify that at this time. Three other RegMap areas were detailed in Noviello et al. (2019), leaving open the potential for future work. Future mappers should also utilize simultaneous information from all images available, even if the area is already thought of as "covered," as additional images could have different imaging parameters that make certain microfeatures more apparent. This is especially important when mapping in areas that don't have corresponding higher-resolution images (≤ 230 m/pix or better).

Finally, the imaging parameters across these four low-resolution images affects the find and accuracy rates for all microfeature types, not just microchaos. The fact that the incidence angles were lower than in the E15RegMap01 images at least partially explains why many of the domes and almost all of the pits were missed, as low incidence angles make it difficult to see topographical variations (Hoppa et al., 2001) or morphology (Greenberg et al., 2003). Under these parameters, the hybrid features, especially the Type II "cracked dome" features, should have also been missed for similar reasons, or at the very least misclassified; this finding has been previously mentioned earlier in this text. Additionally, the typical size of these microfeatures (4–5 km for equal-area diameter and 5–8 km for maximum length) is under the 7.5 km limit, already biasing a mapper against finding them. When combined with the low incidence angles that minimize topographic variations, the fact that domes and pits are found and correctly classified at such low rates is fully understood. Examining low resolution images, or parts of images, with higher incidence angles could change the number and accuracy of pits and domes.

4.4. Phantom features

A final important limit on mapping in low-resolution images is the nature of phantom features in the E15LowRes01 dataset as it constrains how many features mapped in low-resolution imaging are not microfeatures at all and the reasons they were falsely identified. We report a total of 76 phantom features within the 214 features mapped in E15LowRes01 (35.5%), which is actually more features than we correctly classified. Examples of phantom features are shown in Fig. 9. This number initially suggests that a third of features mapped in low-resolution imaging could be non-features in higher resolution images. Eight out of the 76 features were above the 100 km^2 maximum size for microfeature classification, and the remaining 68 features (89.5% of the total phantom features) are examined further to determine common reasons for mapping a featureless area as a feature in E15LowRes01. On numbers alone, that means that 68 out of 187 mapped microfeatures (36.4%) were revealed to be phantom features.

There are specific reasons why false positives are represented in the dataset, as illustrated in Figs. 9 and 10. Most often (27 out of 68 phantom features, 39.7% for phantom microfeatures), a phantom feature was associated with a ridge on Europa, either the shadow of a single ridge or a location where multiple ridges intersect. While all efforts were made to exclude ridges from being misclassified as microfeatures, in low-resolution images with inconsistent lighting, ridges are not always recognizable as such. This is especially true for the thinner ridges (total width less than 2 km) or where dark spots that could indicate a feature jut out perpendicularly to the ridge. Sometimes (16 out of 68 phantom features, 23.5%) there was an anomalous dark spot in otherwise smooth terrain or there was a feature mapped in an area that was full of generally rough (though not fully chaotic) terrain. These dark areas were mistakenly classified as microchaos or spots because of their low apparent albedo. Three times (4.4%), a bright spot within a ridge was mistaken for the bright side of a pit or a dome. Seven times (10.3%) a phantom feature was the shadow of another actual feature, including real microfeatures. The remaining 15 times a potential feature was mapped and turned out to be a featureless area of Europa are true errors. These account for 22.1% of all of the phantom feature areas.

The phantom rate also generally decreases as size increases. A simple linear regression model of the percentage of phantom features versus binned feature areas (y-intercept = 61.67, 95% CI:[43.07, 80.24], p-value <0.001; slope = −0.651, 95% CI:[−0.999, −0.303], p-value = 0.002) shows a strong negative correlation between area of a feature and the phantom feature rate ($r^2 = 0.669$, $r^2_{adj.} = 0.662$, p-value <0.001). As the smallest microfeature type, the spots category is the one most likely to have false positives, though the possibility is present in every feature group to varying degrees (Table 4). Spots are also overrepresented in the E15LowRes01 dataset (Table 3); the 53 spots identified in the

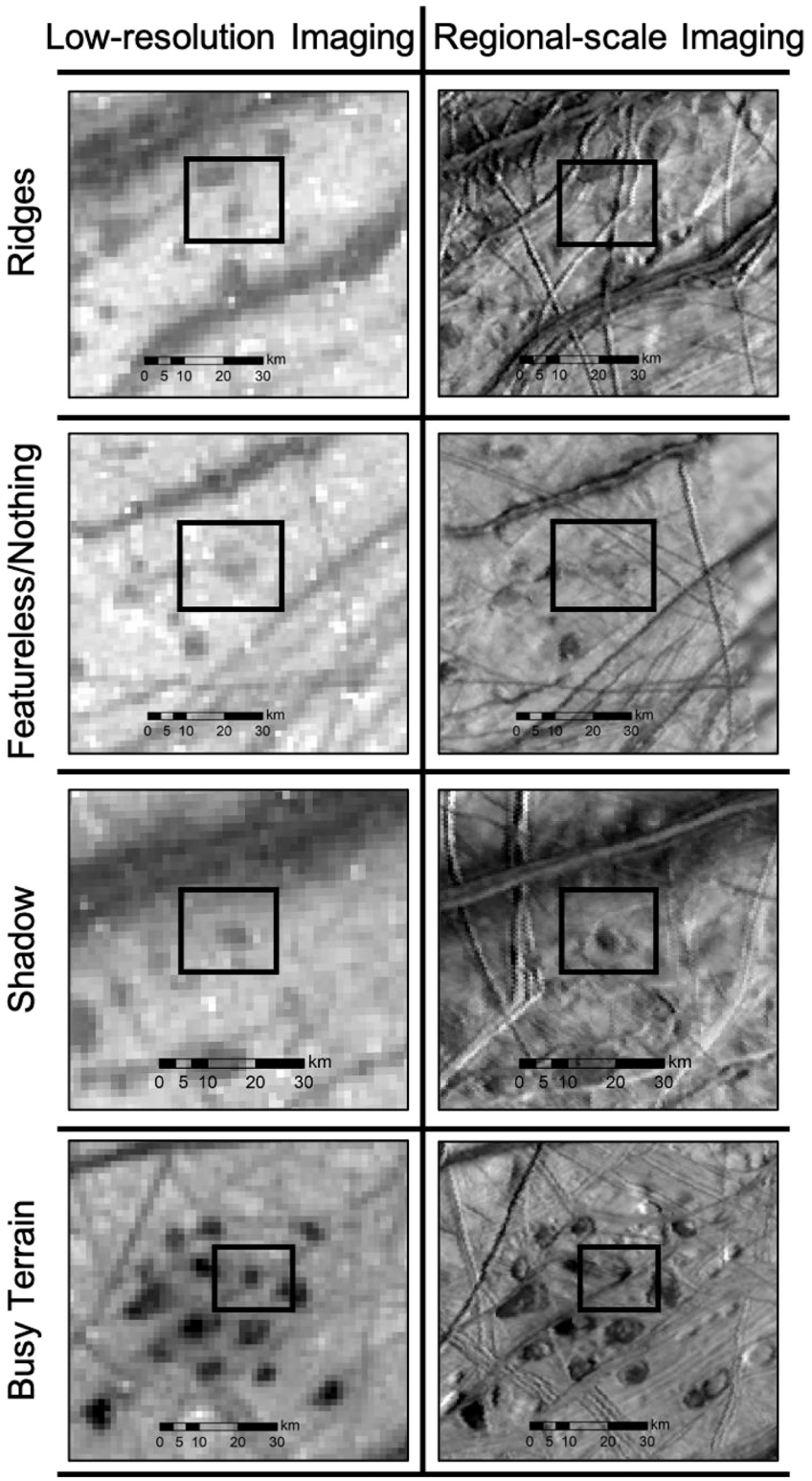

Fig. 9. Multiple examples of phantom features in the dataset broken down into their main categories. On the left are the low-resolution images, and on the right are the regional mosaic images. In the Shadow images, also note how many of the ridges are invisible in the low-resolution imaging. North is up.

E15LowRes01 dataset far exceeds the total number of mapped spots in the E15RegMap01 images. Part of the reason may be that spots, by definition, are discrete areas of consistently low albedo and no visible interior features, a definition that also describes shadows of ridges and other microfeature types whose details are lost in low-resolution images. According to our study, a feature that looks like a spot has a 50% chance of being a false positive, so spots are not reliable datapoints when evaluating global trends on Europa using low-resolution imagery.

4.5. Applications to current global mapping efforts

Based on the features in the E15RegMap01 region, maps of microfeatures within low-resolution images likely miss about 40% of the actual features present in a region; we identified only 117 of the 310

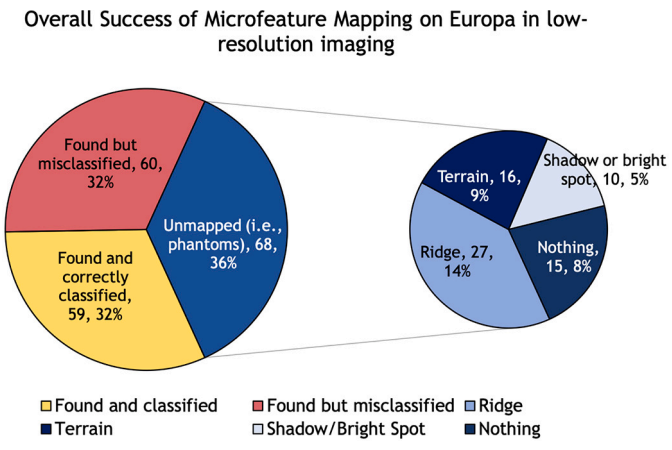

Fig. 10. Left: a pie chart showing the total number of features in E15LowRes01 that were found and correctly classified, found but misclassified, and were unmapped areas (i.e., the phantom features). Right: the phantom features category was broken down further to show the reasons for why these features were mapped if they were not associated with a true microfeature. Percentages represent their percentage shares of the total microfeature number, not the percentage shares of the unmapped features total number. Examples of the phantom features types are shown in Fig. 9.

features mapped by Noviello et al. (2019). Most of the features that can be identified are microchaos, hybrids, or spots, but it is difficult to confidently differentiate between these feature types. Hence, a low resolution global map of microfeatures most likely includes predominantly microchaos, hybrids, and spots, especially the larger ones, and is unlikely to include many domes or any pits. A global map of microfeatures on Europa could map.

Classification is even more challenging in low-resolution. We matched the high-resolution classification for 30% of the features across all feature types, whereas we correctly classified microchaos, hybrid, and spots (when considering them as a single group) 40% of the time. In addition, about 36% of features mapped at low resolution are phantoms. Together, these results suggest that, for a population of e.g., 100 microfeatures mapped in low resolution, up to 40 are not true microfeatures, around 30 are classified correctly, the remaining 30 potential microfeatures are real but misclassified. We can also use these results to estimate how many features are typically missed. Out of 310 mapped in the E15RegMap01 dataset, 187 potential microfeatures were found in low-resolution mapping, a ratio of 1.66:1. Even though some of these were revealed to be phantom features, we must assume that phantom features will be a part of every low-resolution mapping dataset, so this estimate is still appropriate. We can then expect between 60 and 70 other microfeatures in the same area would be missed for images with similar lighting conditions, and that they would mostly be pits and domes.

To fully quantify the likelihood of false positives and missing features within a global data set, additional regions with both high and low resolution images should be analyzed. Of the four areas mapped by Noviello et al. (2019), E15RegMap01 had the highest number of microfeatures, and hence, the largest potential for missed features. Future analysis of sparser regions can provide additional constraints on the appearance of phantom features within low resolution images as there is more surface area available to be misinterpreted.

5. Conclusion

The relative lack of imaging data on Europa confounds efforts to understand the process behind microfeature and chaos formation. Efforts to map microchaos outside of the traditional RegMap areas (Bunte, 2013; Leonard et al., 2019) have been completed, and we have provided some estimates of the uncertainties associated with these maps. Lighting conditions and the subjective approaches between individual mapping datasets can also affect the identification of microchaos and microfeatures in general (Hoppa et al., 2001; Neish et al., 2012).

This work presented a new dataset mapped in low-resolution images covering the same area as a well-studied regional mosaic on the northern, trailing hemisphere of Europa (E15RegMap01) for comparison purposes. E15RegMap01 was selected because it had the highest number of microfeatures in the regional mosaic mapping project as described in Noviello et al. (2019), and thus the most opportunities to find multiple features in low-resolution images. It also provided the most chances for mistakes and the best chance of quantifying those mistakes. This approach is most successful in regions that have not been severely disrupted by large chaotic terrain and chaos features, linear geologic features such as bands and ridges, or areas of proposed tectonic activity (i.e., subsumption; Kattenhorn and Prockter, 2014). These areas are likely to have few microfeatures in general because of large-scale surface modifications, and as the presence of ridges is a significant source of error in mapping, are best avoided for maximal success in microfeature mapping.

An independent dataset was created of the E15RegMap01 region by mapping features in four low-resolution images. Microchaos, spots, and hybrid features were relatively easy to find, while pits and domes were most often missed. Microchaos was also fairly easy to recognize as chaos, and approximately 60% of potential microchaos features were verified as true microchaos in the E15RegMap01 dataset. Hybrids and spots were also found at relatively high rates, but were often confused with each other, and with microchaos. The overall accuracy of only microchaos, hybrids, and spots is roughly 40%. Pits and domes were almost never recognized as pits or domes, and thus have very low accuracy rates. On top of low find rates for both of these feature types (24.2% and 5.0%, respectively), it is fair to say that pits and domes are effectively unidentifiable in low-resolution images.

All microfeatures provide critical information regarding Europa's geologic history and microfeature formation processes, and thus all efforts should seek to be as inclusive as possible when mapping microfeatures. Examining the same areas of Europa under different lighting conditions as much as the *Galileo* imaging dataset allows is the best approach to get an accurate picture of Europa's surface. Present and future global mapping efforts of Europa are likely to be fairly successful in identifying microchaos, hybrids, and spots, but less successful in identifying pits and domes. Using images or parts of images where the incidence angles emphasize topography over albedo (>50° at a minimum) will likely address this issue, though how completely is still an open question.

One warning is that not all dark "chaotic" features in low-resolution images are microchaos, hybrids, or spots. Some of these false positives (phantom features) were associated with ridges, some were associated with the shadows of topographic highs and lows, and some were anomalously dark areas in Europa's plains regions that have no associated microfeature. This false positive rate could be as high as 36%, roughly 1 in 3 mapped features. Europa mappers should take care to avoid ridges as much as possible to minimize the risk of mapping phantom features, though it will not eliminate the risk entirely. Future low-resolution mapping studies of Europa should also be aware that features larger than 5 km in diameter are significantly more valuable for making global inferences regarding Europa than features below 5 km. This number is a moderate value between the smallest feature that was correctly identified (a 3.56 km spot) and the five pixel limit (7.5 km), though it is ultimately up to the mapper how conservative they will be. By only considering features above 5 km, the likelihood that the feature is a true microfeature as opposed to a phantom feature and the likelihood that the feature has been correctly classified increases. This does not mean that smaller features should be completely disregarded, but any general interpretation should minimally rely on them.

The findings presented here suggest that there are many more places

where potential microfeatures could be mapped on Europa's surface, thus dramatically increasing the amount of information available on microfeatures and providing solid constraints for modeling studies (Collins and Nimmo, 2009; Schmidt et al., 2011; Michaut and Manga, 2014; Manga and Michaut, 2017). The ultimate extension of this work would be a map of all chaos, micro- and otherwise, with a confidence level attached to all the features represented on the map. These robust observations would provide firm limitations that need to be explained by microchaos and microfeature formation models, in turn advancing the state of knowledge of Europa's geophysics, heat and material transport processes, and surface evolution. This work will also allow for predictions to be made ahead of the Europa Clipper Flagship mission (Phillips and Pappalardo, 2014; Pappalardo et al., 2016; Pappalardo et al., 2017) regarding Europa's geology, which can then be tested with the instrument data from the mission.

Declaration of Competing Interest

None.

Acknowledgements

This work was partially supported by NASA grant NNX15AH91G. J. L. Noviello would like to thank David Nelson of ASU for his efforts and teachings on ISIS3 and ArcGIS, Meg Burris of ASU for her help on figures, Cynthia Phillips of JPL for her help on interpreting the *Galileo* imaging records, and David A. Williams of ASU and Patrick Gasda of Los Alamos National Laboratory for helpful feedback on drafts of the manuscript. A. Rhoden wishes to thank E. M. Huff of JPL and G. C. Collins of Wheaton College for useful discussions that contributed to this work. We both thank the three anonymous reviewers for their insightful and constructive comments that greatly improved this work. This research has made use of the USGS Integrated Software for Imagers and Spectrometers (ISIS3) and the USGS Planetary Image Locator Tool (PILOT) image finder.

Supplementary data

Supplementary data to this article can be found online at https://doi.org/10.1016/j.icarus.2021.114495.

References

Anderson, J.A., et al., 2004. Modernization of the integrated software for imagers and spectrometers, lunar planet. In: Sci. XXXV, Houston, Texas, abstract #2039.
Belton, M.J.S., et al., 1992. The Galileo solid-state imaging experiment. Space Sci. Rev. 60, 413–455.
Bunte, M.K., 2013. Utilizing Science and Technology to Enhance a Future Planetary Mission: Applications to Europa. Ph.D. thesis. Arizona State University, Tempe, Arizona (279 pp).
Carr, M.H., et al., 1998. Evidence for a subsurface ocean on Europa. Nature 391, 363–365. https://doi.org/10.1038/34857.
Chyba, C.F., Phillips, C.B., 2007. Europa. In: Sullivan III, W.T., Barross, J.A. (Eds.), Planets and Life: The Emerging Science of Astrobiology. Cambridge Univ. Press, Cambridge, UK, pp. 388–423.
Collins, G.C., Head, J.W., Pappalardo, R.T., Spaun, N.A., 2000. Evaluation of models for the formation of chaotic terrain on Europa. J. Geophys. Res. 105, 1709–1716.
Collins, G., Nimmo, F., 2009. Chaotic Terrain on Europa. In: Pappalardo, R.T., McKinnon, W.B., Khurana, K.K. (Eds.), Europa. The University of Arizona Press, pp. 259–281.
Craft, K.L., Patterson, G.W., Lowell, R.P., Germanovich, L., 2016. Fracturing and flow: investigations on the formation of shallow water sills on Europa. Icarus 274, 297–313.
Culha, C., Manga, M., 2016. Geometry and spatial distribution of lenticulae on Europa. Icarus 271, 49–56.
Doggett, T., Greeley, R., Figueredo, P., Tanaka, K., 2009. Geologic Stratigraphy and Evolution of Europa's Surface. In: Pappalardo, R.T., McKinnon, W.B., Khurana, K.K. (Eds.), Europa. The University of Arizona Press, pp. 137–159.
Fanale, F.F., Granahan, J.C., Greeley, R., et al., 2000. Tyre and Pwyll: Galileo orbital remote sensing onf mineralogy versus morphology and two selected sites on Europa. J. Geophys. Res. 105, 22647–22655.
Figueredo, P.H., Greeley, R., 2004. Resurfacing history of Europa from pole-to-pole geological mapping. Icarus 167, 287–312.
Figueredo, P.H., Chuang, F.C., Rathbun, J., Kirk, R.L., Greeley, R., 2002. Geology and origin of Europa's "mitten" feature (Murias Chaos). J. Geophys. Res. 107 https://doi.org/10.1027/2001JE001591.
Geissler, P.E., Greenberg, R., Hoppa, G., et al., 1998. Evidence for non-synchronous rotations on Europa. Nature 391, 368–370.
Greeley, R., et al., 2000. Geologic mapping of Europa. J. Geophys. Res. 105, 22559–22578.
Greenberg, R., Hoppa, G.V., Tufts, B.R., Geissler, P., Riley, J., Kadel, S., 1999. Chaos on Europa. Icarus 141, 263–286.
Greenberg, R., Leake, M.A., Hoppa, G.V., Tufts, B.R., 2003. Pits and uplifts on Europa. Icarus 161, 102–126.
Hand, K.P., Carlson, R.W., 2015. Europa's surface color suggests an ocean rich with sodium chloride. Geophys. Res. Lett. 42, 3174–3178.
Hoppa, G.V., Greenberg, R., Riley, J., Tufts, B.R., 2001. Observational selection effects in Europa image data: identification of chaotic terrain. Icarus 151, 181–189.
Kattenhorn, S., Prockter, L.M., 2014. Evidence for subduction in the ice shell of Europa. Nat. Geosci. 7, 762–767.
Leonard, E.J., Senske, D., Patthoff, D.A., 2019. Global and Regional scale Geologic Mapping on Europa. European Planetary Science Conference/Division of Planetary Sciences Joint Meeting, Geneva, Switzerland, Abstract #57–1.
Manga, M., Michaut, C., 2017. Formation of lenticulae on Europa by saucer-shaped sills. Icarus 286, 261–269.
Michaut, C., Manga, M., 2014. Domes, pits, and small chaos on Europa produced by water sills. J. Geophys. Res. 119, 550–573. https://doi.org/10.1002/2013JE004558.
Mitri, G., Showman, A.P., 2008. A model for the temperature-dependence of tidal dissipation in convection plumes on icy satellites: implications for Europa and Enceladus. Icarus 195, 758–764.
Neish, C.D., Prockter, L.M., Patterson, G.W., 2012. Observational constraints on the identification and distribution of chaotic terrain on icy satellites. Icarus 221, 72–79.
Noviello, J.L., Torrano, Z.A., Rhoden, A.R., Singer, K.N., 2019. Mapping Europa's microfeatures in regional mosaics: new constraints on formation models. Icarus 329, 101–123.
Pappalardo, R.T., Barr, A.C., 2004. The origin of domes on Europa: the role of thermally induced compositional diapirism. Geophys. Res. Lett. 31 https://doi.org/10.1029/2003GL019202.
Pappalardo, R.T., Sullivan, R.J., 1996. Evidence for separation across a gray band on Europa. Icarus 123, 557–567.
Pappalardo, R.T., et al., 1998. Geological evidence for solid-state convection in Europa's ice shell. Nature 391, 365–368.
Pappalardo, R.T., et al., 2016. Science objectives and capabilities of the NASA Europa mission. In: Lunar planet. Sci. XLVII, Houston, Texas, abstract #3058.
Pappalardo, R.T., et al., 2017. The Europa clipper Mission: exploring the habitability of a unique icy world. In: European planet. Sci. Congress 11, abstract #304.
Phillips, C.B., Pappalardo, R.T., 2014. Europa clipper Mission concept: exploring Jupiter's ocean moon. Eos 95, No. 20, pp. 165–167.
Prockter, L.M., Antman, A.M., Pappalardo, R.T., et al., 1999. Europa: stratigraphy and geological history of the anti-jovian region from Galileo E14 solid-state imaging data. J. Geophys. Res. 104, 16531–16540.
Prockter, L.M., Shirley, J.H., Dalton III, J.B., Kamp, L., 2017. Surface composition of pull-apart bands in Argadnel Regio, Europa: evidence of localized cryovolcanic resurfacing during basin formation. Icarus 285, 27–42. https://doi.org/10.1016/j.icarus.2016.11.024.
Rathbun, J.A., Musser, G.S., Squyres, S.W., 1998. Ice diapirs on Europa: implications for liquid water. Geophys. Res. Lett. 25, 4157–4160.
Riley, J., Hoppa, G.V., Greenberg, R., Tufts, B.R., Geissler, P., 2000. Distribution of chaotic terrain on Europa. J. Geophys. Res. 105, 22599–22615.
Schmidt, B.E., Blankenship, D.D., Patterson, G.W., Schenk, P.M., 2011. Active formation of 'chaos terrain' over shallow subsurface water on Europa. Nature 479, 502–505.
Showman, A.P., Han, L., 2005. Effects of plasticity of convection in Europa's ice shell: implications for surface features. Icarus 177, 425–437.
Singer, K.N., McKinnon, W.B., Schenk, P.M., 2010. Pits, spots, uplifts, and small chaos regions on Europa: evidence for diapiric upwelling from morphology and morphometry. In: Lunar planet. Sci. XLI, Houston, Texas, abstract #2195.
Singer, K.N., McKinnon, W.B., Schenk, P.M., 2013. Pits, Uplifts and Small Chaos Features on Europa: Evidence for Diapiric Upwelling from Morphology and Morphometry (In revisions at Icarus).
Soderlund, K.M., Schmidt, B.E., Wicht, J., Blankenship, D.D., 2014. Ocean-driven heating of Europa's icy shell at low latitudes. Nat. Geosci. 7, 16–19. https://doi.org/10.1038/NGEO02021.
Sotin, C., Head, J.W., Tobie, G., 2002. Europa: Tidal heating of upwelling thermal plumes and the origin of lenticulae and chaos melting. Geophys. Res. Lett. 29.
Spaun, N., Head, J., Collins, G., Prockter, L., Pappalardo, R., 1998. Conamara Chaos region, Europa: reconstruction of mobile polygonal ice blocks. Geophys. Res. Lett. 25, 4277–4280.
Spaun, N., Head, J., Pappalardo, R., the Galileo SSI Team, 1999. Chaos and lenticulae on Europa: Structure, morphology and comparative analysis. Lunar Planet. Sci. XXX, Houston, Texas, Abstract #1276.
Torson, J.M., Becker, K.J., 1997. ISIS - a software architecture for processing planetary images, lunar planet. Sci. XXVIII, Houston, Texas, abstract #1219.
U.S. Geological Survey, 2002. Controlled photomosaic map of Europa, Je15M CMN: U.S. Geological Survey Geologic Investigations Series I–2757 available at. http://pubs.usgs.gov/imap/i2757/.
U.S. Geological Survey, 2020. PILOT - the planetary image locator tool.